Screening, Hyperuniformity, and Instability in the Sedimentation of Irregular Objects

Tomer Goldfriend*
Raymond & Beverly Sackler School of Physics and Astronomy, Tel Aviv University, Tel Aviv 69978, Israel

Haim Diamant†
Raymond & Beverly Sackler School of Chemistry, Tel Aviv University, Tel Aviv 69978, Israel

Thomas A. Witten‡
Department of Physics and James Franck Institute, University of Chicago, Chicago, Illinois 60637, USA
(Received 26 December 2016; published 14 April 2017)

We study the overdamped sedimentation of non-Brownian objects of irregular shape using fluctuating hydrodynamics. The anisotropic response of the objects to flow, caused by their tendency to align with gravity, directly suppresses concentration and velocity fluctuations. This allows the suspension to avoid the anomalous fluctuations predicted for suspensions of symmetric spheroids. The suppression of concentration fluctuations leads to a correlated, hyperuniform structure. For certain object shapes, the anisotropic response may act in the opposite direction, destabilizing uniform sedimentation.

DOI: 10.1103/PhysRevLett.118.158005

Sedimentation, the settling of colloidal objects under gravity, is a fundamental and ubiquitous physical process whose details are still under debate (see the reviews in Refs. [1,2]). The related process of bed fluidization is widely used in reactors, filtration, and water treatment [3]. Long-range hydrodynamic correlations among settling objects lead to complex many-body dynamics, exhibiting strong fluctuations and large-scale dynamic structures even for athermal (non-Brownian) objects with negligible inertia [4–7]. One of the key issues is the extent of velocity fluctuations of the sedimenting objects about their mean settling velocity. A famous prediction by Caflisch and Luke [8] stated that the magnitude of the velocity fluctuations of individual objects should diverge with system size. Over the years there has been evidence from theory and simulations both in favor of [9–14] and against [1,15–17] this prediction. Experimentally, the indefinite growth of velocity fluctuations with system size has not been observed [5,6].

To resolve the Caflisch-Luke paradox, several screening mechanisms have been suggested: a characteristic screening length emerging from correlations between concentration fluctuations (the structure factor of the suspension) [15], e.g., as a result of stratification [14,18], inertial effects [17], side-wall effects [17]; and noise-induced concentration fluctuations [1,16].

Earlier theories have considered symmetric objects, mostly spheres. Spheroids [19,20], rodlike objects [21–27], and permeable spheres [28] were studied as well. In various scenarios, including applications involving fluidized beds, the suspensions contain objects of asymmetric shapes. In the present work we address the sedimentation of a large class of irregular objects that are self-aligning [29]. Under gravity, in addition to settling, such an individual object aligns an eigendirection with the driving force. This should be distinguished from symmetric objects like rods, which align with flow lines [19,23] rather than with an external force of fixed direction. In general, these objects are chiral and thus also rotate about the force direction in a preferred sense of rotation. Both the eigendirection and angular velocity are determined by the object's geometry and mass distribution [29]. The hydrodynamic pair interactions between self-aligning objects have been studied in Refs. [30,31]. Unlike spheres, the objects respond anisotropically to nonuniform flow. This fact, as shown below, suppresses fluctuations for arbitrarily weak inhomogeneity (unlike the case of spheres studied in Ref. [16]).

We begin with a qualitative description of the effects studied here. Consider a suspension of objects sedimenting in a viscous fluid of viscosity η under a force F in the $-z$ direction. The mean concentration is c_0. Let us imagine a sinusoidal variation $c(x)$ about c_0, of wavelength λ, in the transverse x direction, creating vertical slabs of heavier and lighter weights. This creates a velocity variation $U(x)$. To find the amplitude of this variation we balance the change in gravitational force with the change in viscous drag (per unit area of the slab), $c\lambda F \sim \eta U/\lambda$, resulting in $U \sim c\lambda^2 F/\eta$. This indefinite increase of U with λ is a manifestation of the Caflisch-Luke problem. The relative velocity of the slabs creates a vorticity ω of order $U/\lambda \sim c\lambda F/\eta$. For spheres, this vorticity merely rotates the objects. Self-aligning objects, by contrast, are tilted away from their aligned state. Their misalignment, proportional to ω, makes them glide in the x direction with velocity $U_\perp \sim \gamma a c\lambda F/\eta$, where a is the size of the object and γ a proportionality coefficient. The time derivative of concentration, arising from the gradient of flux, reads $\dot{c} \sim -c_0 U_\perp/\lambda = -(\gamma a c_0 F/\eta)c$. Now, if the coefficient γ is positive, the response suppresses the inhomogeneity, whereas if it is negative the inhomogeneity is enhanced. This is a mechanism of either screening or instability. In addition, the independence of the last relation on λ implies (for $\gamma > 0$) a nondiffusive fast relaxation over large length scales. As shown below, this leads to a hyperuniform dynamic structure. By equating the diffusive and nondiffusive relaxation rates of a slab, $D\lambda^{-2} = \gamma a c_0 F/\eta$, where D is the hydrodynamic diffusion coefficient, we find a typical wavelength above which hyperuniformity sets in, $\xi = [\gamma a c_0 F/(\eta D)]^{-1/2}$. Note that the mechanism just described does not work for concentration variations in the z direction [32].

To study these effects in more detail we use the framework of fluctuating hydrodynamics. Similar continuum approaches were used for spheres by Levine, Ramaswamy, Frey, and Bruinsma (LRFB) [16], and by Mucha *et al.* [14]. We consider an athermal inertialess suspension. The system depends on the following parameters: the gravitational force on a single object F, the solvent viscosity η, the characteristic size of the objects a, and the mean concentration of objects c_0. In addition, a self-aligning object has an alignability parameter α, giving the slowest relaxation rate of a misaligned orientation toward alignment, $\tau_{\mathrm{align}}^{-1} = \alpha F/(\eta a^2)$ [29]. This parameter is derivable from the object's shape and mass distribution alone.

The stochastic response of the suspension is characterized by a phenomenological diffusion coefficient D, measurable in experiments [4], and fluctuating object fluxes $\mathbf{f}(\mathbf{r}, t)$, treated as a Gaussian white noise with variance $\langle f_i(\mathbf{r}, t) f_j(\mathbf{r}', t')\rangle = 2c_0 N\delta_{ij}\delta(\mathbf{r}-\mathbf{r}')\delta(t-t')$ [1,16]. The parameters D and N, which originate in the complex many-body interactions excited by the force F at each object, are in general anisotropic [4,16,33]. Yet, unlike the LRFB model, the effects discussed below do not depend crucially on this anisotropy; we therefore neglect it for the sake of simplicity. In addition, D may depend on the volume fraction due to shear-induced diffusion [34]. As this dependence was experimentally found to be weak [4,33], we neglect it as well.

We employ the following three additional assumptions. (1) The suspension is dilute, having a volume fraction $\varphi \ll 1$, such that direct interactions between the objects are negligible, and the hydrodynamic interaction is well described by its two leading multipoles. (2) The suspension is non-Brownian, i.e., the thermal Péclet number $Fa/(k_B T) \gg 1$, where $k_B T$ is the thermal energy. However, there is no restriction on the sedimentation Péclet number, defined as $\mathrm{Pe} \equiv F/(\eta D)$. (3) We assume strong alignability, i.e., that the rate of alignment, $\tau_{\mathrm{align}}^{-1}$, is much faster than the interaction-induced vorticity $\omega \sim 1/(\eta l^2)$, where $l \sim a\varphi^{-1/3}$ is the typical distance between objects. The resulting criterion $\alpha \gg \varphi^{2/3}$ improves with dilution.

The advection-diffusion equation for the fluctuations of object concentration about c_0, $c(\mathbf{r}, t)$, reads

$$\partial_t c + \nabla\cdot[(c + c_0)\mathbf{U}] = D\nabla^2 c + \nabla\cdot\mathbf{f}, \tag{1}$$

where $\mathbf{U}$ is the objects' velocity fluctuation field about the mean settling velocity. The velocity fluctuation of the fluid surrounding the objects, $\mathbf{v}(\mathbf{r}, t)$, is described by an incompressible, overdamped Stokes flow, with force monopoles originating from concentration fluctuations [35],

$$\begin{aligned} v_i(\mathbf{r}, t) &= \int d^3r' G_{ij}(\mathbf{r}-\mathbf{r}')c(\mathbf{r}', t)F_j(\mathbf{r}') + O(a) \\ &= -F\int d^3r' G_{iz}(\mathbf{r}-\mathbf{r}')c(\mathbf{r}', t) + O(a). \end{aligned} \tag{2}$$

Here, $G_{ij}(\mathbf{r}) = (8\pi\eta r)^{-1}(\delta_{ij} + r_i r_j/r^2)$ is the Green's function of Stokes flow (the Oseen tensor) [36].

A pointlike object ($a \to 0$) is merely advected by the flow, i.e., $\mathbf{U} = \mathbf{v}$. However, for nonzero a the two velocities do not coincide. To leading order in a they are bound to satisfy a relation of the form

$$U_i = v_i + a\Phi_{ikj}\partial_j v_k + O(a^2). \tag{3}$$

The constant tensor $\mathbf{\Phi}$ depends on the objects' orientations and shapes, and is assumed to be independent of c [37]. The difference between $\mathbf{U}$ and $\mathbf{v}$, and the fact that the effective response Φ is anisotropic, lead to a new advective term in Eq. (1), which corresponds to an object flux with nonzero divergence, $\partial_i U_i = a\Phi_{ikj}\partial_i\partial_j v_k + O(a^2) \neq 0$. The second term in Eq. (3) is at the core of the present theory; the existence of asymmetry in Φ_{ikj}, demanded phenomenologically for self-aligning objects, entails the effects described below [for spheres the second term in Eq. (3) vanishes, and the higher-order terms are divergenceless]. The anisotropic response has two contributions: one from a direct translational response to shear flow, and the other due to the object's gliding response mentioned above [38].

We proceed by substituting Eqs. (2) and (3) into Eq. (1) and Fourier transforming the resulting equation $[(\mathbf{r}, t) \to (\mathbf{q}, \omega)]$. This leads to

$$\begin{aligned} &-i\omega\tilde{c}(\mathbf{q}, \omega) + \frac{c_0 a F}{\eta}\left(\gamma\frac{q_\perp^2}{q^2} + \bar{\gamma}\frac{q_\perp^4}{q^4}\right)\tilde{c}(\mathbf{q}, \omega) \\ &\quad + iF\int q_i\tilde{G}_{i3}(\mathbf{q}')\tilde{c}(\mathbf{q}-\mathbf{q}', \omega-\omega')\tilde{c}(\mathbf{q}', \omega')d^3q' d\omega' \\ &\qquad = -Dq^2\tilde{c}(\mathbf{q}, \omega) - i\mathbf{q}\cdot\tilde{\mathbf{f}}(\mathbf{q}, \omega), \end{aligned} \tag{4}$$

where we used the fact that $q_i'\tilde{G}_{ij}(\mathbf{q}') = 0$. We denote by $\perp$ the horizontal components (x, y) of a vector. The coefficients γ and $\bar{\gamma}$ are effective response parameters resulting from the response tensor Φ (specifically, $\gamma = \Phi_{zzz} - \Phi_{z\perp\perp} - \Phi_{\perp\perp z}$, $\bar{\gamma} = \Phi_{\perp\perp z} + \Phi_{\perp z\perp} + \Phi_{z\perp\perp} - \Phi_{zzz}$). The second term in Eq. (4) corresponds to linear screening, which is nonzero for any wave vector $\mathbf{q} \nparallel \hat{\mathbf{z}}$. This term makes a simple perturbation theory in small concentration fluctuations valid, allowing us to neglect the third, nonlinear term that underlies the LRFB model. In addition, to facilitate the analysis, we omit the term proportional to $\bar{\gamma}$, which does not affect the following calculations. We thus have

$$-i\omega\tilde{c}(\mathbf{q},\omega)+\gamma\frac{c_0aF}{\eta}\frac{q_\perp^2}{q^2}\tilde{c}(\mathbf{q},\omega)$$
$$=-Dq^2\tilde{c}(\mathbf{q},\omega)-i\mathbf{q}\cdot\tilde{\mathbf{f}}(\mathbf{q},\omega). \qquad (5)$$

By equating the diffusive and screening terms in Eq. (5), we obtain the characteristic length that we qualitatively inferred above

$$\xi=\left(\frac{\gamma c_0 aF}{\eta D}\right)^{-1/2}=a\gamma^{-1/2}\varphi^{-1/2}\mathrm{Pe}^{-1/2}. \qquad (6)$$

Results.—We now summarize the main results, which are readily obtained from Eqs. (2)–(5). We begin with the expressions for the concentration and velocity correlation functions at steady state ($\omega\to 0$):

$$S(\mathbf{q})=\langle\tilde{c}(\mathbf{q},0)\tilde{c}(-\mathbf{q},0)\rangle=\frac{N}{D}\frac{q^2}{q^2+\xi^{-2}(q_\perp/q)^2}, \qquad (7)$$

$$\langle\tilde{U}_i(\mathbf{q},0)\tilde{U}_j(-\mathbf{q},0)\rangle=\frac{NF^2}{D}\frac{\tilde{G}_{iz}(\mathbf{q})\tilde{G}_{jz}(-\mathbf{q})q^2}{q^2+\xi^{-2}(q_\perp/q)^2}, \qquad (8)$$

where $S(\mathbf{q})$ is the static structure factor of the suspension. Figure 1(a) shows $S(\mathbf{q})$ along different directions of $\mathbf{q}$. The structure factor decays to zero at small q, as q^2, in all directions except $\hat{\mathbf{z}}$, where it is a constant at small q. Next, the velocity point-correlation functions are obtained by inverting back to real space and taking the limit $r\to 0$,

$$\langle U_z^2(0)\rangle=6\langle U_\perp^2(0)\rangle=\frac{3}{64}\varphi\frac{N}{D}\frac{\xi}{a}\left(\frac{F}{\eta a}\right)^2$$
$$=\frac{3}{64}\frac{N}{D}\left(\frac{D}{a}\right)^2\gamma^{-1/2}\varphi^{1/2}\mathrm{Pe}^{3/2}. \qquad (9)$$

Finally, we give the asymptotic expressions at large distances ($r\gg\xi$) for the two-point correlations in real space. For the concentration correlations we get

$$\frac{D\xi^3}{c_0N}\langle c(0)c(r\hat{\mathbf{z}})\rangle=\frac{12}{\pi}\frac{\xi^5}{r^5},$$
$$\frac{D\xi^3}{c_0N}\langle c(0)c(r\hat{\mathbf{r}}_\perp)\rangle=\frac{\Gamma^2(5/4)}{2\sqrt{2}\pi^2}\frac{\xi^{5/2}}{r^{5/2}}, \qquad (10)$$

where Γ is the gamma function. The weaker decay $\sim r^{-5/2}$ applies strictly within the (x,y) plane. For the velocity correlations we get

$$C_{\perp\perp}(r\hat{\mathbf{z}})=\frac{8\xi^3}{\pi r^3},\qquad C_{\perp\perp}(r\hat{\mathbf{r}}_\perp)=\frac{\xi}{\pi r}, \qquad (11)$$

$$C_{zz}(r\hat{\mathbf{z}})=\frac{4\xi}{\pi r},\qquad C_{zz}(r\hat{\mathbf{r}}_\perp)=\frac{2\xi}{\pi r}, \qquad (12)$$

where $C_{ij}(\mathbf{r})\equiv\langle U_i(0)U_j(\mathbf{r})\rangle/\langle U^2(0)\rangle$. Despite the emergence of the characteristic length ξ, the concentration and velocity correlations remain long ranged, decaying algebraically with distance. In Fig. 1(b) we present the spatial correlations at steady state along with their asymptotic power laws.

Discussion.—Let us now discuss the consequences of these results. The velocity autocorrelation of an object is given, up to corrections of $O(a/\xi)$, by the point correlation of Eq. (9). From this expression we immediately see how the finite ξ regularizes the velocity autocorrelations, thus removing the Caflisch-Luke problem [8] for the irregular objects considered here. Indeed, in the limit $\gamma\to 0$ (no self-alignment) the autocorrelation diverges, requiring a different regularization mechanism [14,16]. Figure 2 illustrates another view of the physical mechanism behind the regularization [46]. A concentration fluctuation within a small volume of the suspension creates a flow, which advects objects in and out of the region. Spherical objects respond to the flow isotropically, leading to mutual cancellation of the influx and outflux [Fig. 2(a)]. The dipolar, nondivergenceless flow of irregular objects, as described by Eq. (3), perturbs this balance, compensating for the deficiency or surplus of objects in the region [Fig. 2(b)].

As a simple example we treat the specific shape of self-aligning spheroids, i.e., spheroids whose center of mass is displaced from their centroid; see inset of Fig. 3(a). The corresponding response parameter γ is shown in Fig. 3(a) as a function of the spheroid's aspect ratio κ and the off-center position of the forcing point χ. As the offset χ is reduced, the object is more easily tilted by the flow, thus strengthening the suppression [Fig. 3(a)]. At the same time, however, the object becomes less alignable. Since our calculation is linear in the tilt [38], i.e., it assumes strong alignability, it becomes invalid before the case of a symmetric spheroid ($\chi\to 0$) is reached. The unshaded area in Fig. 3(b) indicates this rough validity regime, which involves also the volume fraction φ. The boundary of this regime gives, roughly, the parameters corresponding to maximum suppression (maximum γ).

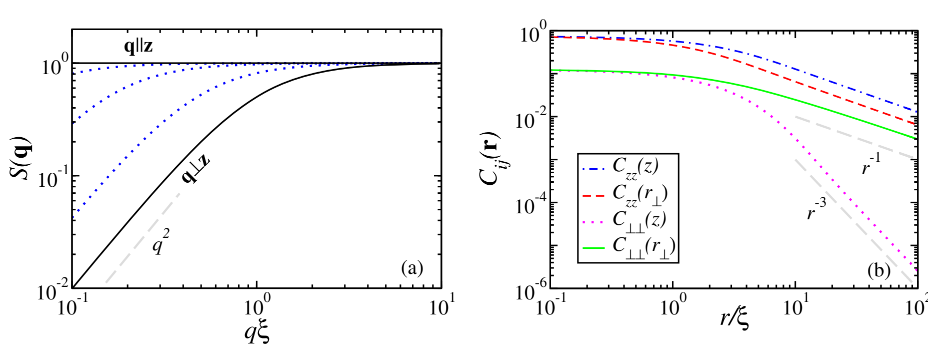

FIG. 1. (a) Static structure factor of the suspension [Eq. (7) with $N=D$]. The blue dotted curves, which correspond to different $\mathbf{q}\nparallel\hat{\mathbf{z}}$, decay to zero at small q as $\sim q^2$. (b) Normalized two-point velocity correlations, together with their asymptotic behavior [Eqs. (11) and (12)].

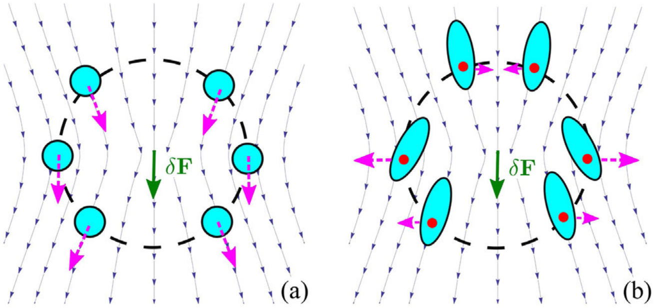

FIG. 2. Illustration of the mechanism regulating concentration fluctuations. A concentration fluctuation makes a force fluctuation $\delta\mathbf{F}$ (green solid arrow), which in turn creates a flow fluctuation (flow lines). (a) Spherical objects respond isotropically to this flow, with velocities (magenta dashed arrows) along the direction of the flow lines; thus, there is no net flux of objects into the small volume element around the fluctuation. (b) Self-aligning spheroids have an anisotropic response, leading in this example to a total outflux of objects. The resulting flow of objects has a nonzero divergence, which reduces the concentration fluctuations.

In all of the above we have implicitly assumed that the effective response parameter γ is positive, leading to a positive ξ^2. As $\gamma \to 0^+$, the characteristic length ξ becomes indefinitely large. In fact, γ may be of either sign, as we now show for self-aligning spheroids [38]. The response parameter resulting from this calculation, shown in Fig. 3(a), reveals a region of negative γ as a function of the spheroid's aspect ratio κ. As is clear from the mechanism described above (Fig. 2), a negative γ implies deregularization, i.e., instability in the sedimentation of such objects, with unstable structures of size $\sim\sqrt{-\xi^2}$. The instability clearly calls for additional theoretical and experimental studies.

As described by Eq. (7) and Fig. 1(a) (in the case of positive γ), for any wave vector $\mathbf{q} \nparallel \hat{\mathbf{z}}$ the structure factor decays to zero for small wave vectors as $S(\mathbf{q}) \sim q^2$. This implies hyperuniformity of the fluctuating suspension [47,48] in any direction but $\hat{\mathbf{z}}$. Calculating the fluctuation δN in the number of objects within a spherical subvolume of radius R, we find $\delta N^2 \sim R^3(R/\xi)^{-1}$, i.e., a variance that grows as the surface area rather than the volume [48]. The hyperuniformity is also manifest in the long-range concentration correlations in the transverse direction, as given in Eq. (10). In the $\hat{\mathbf{z}}$ direction $S(\mathbf{q})$ is constant for small q, implying normal Poissonian fluctuations. The angular dependence of the suppression has been qualitatively explained above. For $q \neq q_z$ and $q < \xi^{-1}$ the vorticity-tilt effect (with rate $D\xi^{-2}$) dominates diffusion (with the slower rate Dq^2), while for $q = q_z$ this effect is absent. Several systems exhibiting hyperuniformity have been recently studied [47,49–51]. Our system is different in several essential aspects: (1) it is dynamic, corresponding to continually changing configurations rather than a static absorbing state; (2) it does not require tuning of a control parameter to a critical value; (3) rather than eliminating collisions, it suppresses both positive and negative concentration fluctuations [52].

It has been assumed for simplicity that all the objects are identical, but the qualitative conclusions apply in more general scenarios. The key requirement is that the system contains self-aligning objects, possessing the dipolar anisotropic response treated above. Not all the objects in the suspension need to be self-aligning, and the self-aligning ones do not need to be identical. In any of these scenarios they will tilt and glide in response to the nonuniform flow, thus producing the suppression or instability mechanisms discussed here.

We now compare our screening mechanisms with the ones suggested for the sedimentation of spheres. Those theories also yielded suppression of fluctuations, but out of different physics. (Indeed, hyperuniformity was found in numerical simulations [53] and experiments [54] of sedimenting spheres.) In the theory of Ref. [16] the effects result self-consistently from the nonlinear coupling between

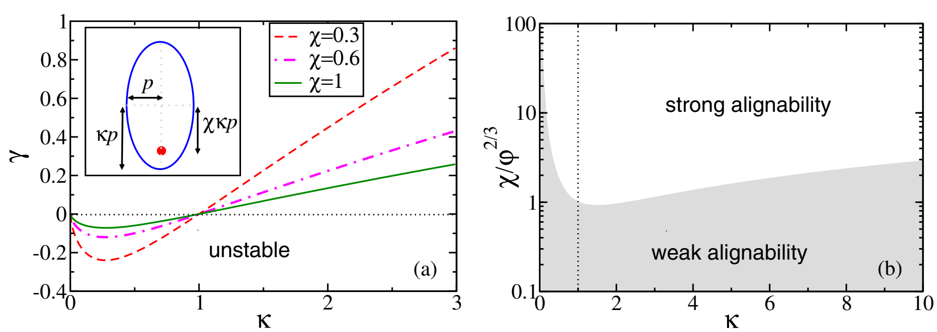

FIG. 3. (a) Effective response parameter γ describing suppressed fluctuations for $\gamma > 0$ as predicted for sedimentation of self-aligning spheroids (inset). The spheroid's response is calculated as a function of its geometry, characterized by the aspect ratio κ, and the displacement of the forcing point (red dot) from the centroid, given by $\chi\kappa p$. Here, $p = \kappa^{-1/3}a$ is the spheroid's minor axis. Prolate self-aligning spheroids ($\kappa > 1$) cause suppression. For spheres ($\kappa \to 1$) our suppression mechanism disappears ($\gamma \to 0$). For $\kappa < 1$ the response parameter γ becomes negative so that the uniform suspension becomes unstable. (b) Validity region of the present theory for self-aligning spheroids. The offset χ should be larger than $\varphi^{2/3}h(\kappa)$ [where the function $h(\kappa)$ is given in the Supplemental Material [38]] to ensure the assumed strong alignability.

concentration and velocity fluctuations, giving $\xi_{\mathrm{LRFB}} \sim a\varphi^{-1/3}\mathrm{Pe}^{-2/3}$. A related study [1,55] suggests that the spherical objects might self-organize into structures that glide similarly to our self-aligning objects. The mechanism of Ref. [14] relies on a steady concentration gradient (stratification), yielding $\xi_{\mathrm{strat}} \sim a\varphi^{-1/4}\mathrm{Pe}^{-1/4}$. Which of these is the actual screening mechanism for spheres remains an open question. If the LRFB mechanism is the one that operates for spheres, then, for asymmetric objects, our linear mechanism with $\xi = a\gamma^{-1/2}\varphi^{-1/2}\mathrm{Pe}^{-1/2}$ should replace the nonlinear one; the linear glide solution is perturbatively stable against the nonlinear term at steady state [38]. If stratification is the active mechanism for spheres, then screening will be caused by a combination of both stratification and asymmetry. Another distinctive feature of the asymmetry mechanism is that it remains in place as the system approaches detailed balance ($D = N$), whereas the LRFB screening disappears [16]. Thus, we expect the present mechanism to hold for an arbitrarily small sedimentation Péclet number (while keeping the thermal Pe large).

Conclusion.—The findings presented above for asymmetric dispersions can be checked experimentally, e.g., using light scattering or video microscopy. Our results highlight the different physics underlying the sedimentation of irregular objects as compared to spheroidal ones. This includes a distinctive, direct, screening mechanism, a different length scale ξ beyond which hyperuniformity sets in, and unstable dynamics for certain object shapes. These results may offer new means of controlling the stability of driven suspensions such as fluidized beds.

We thank P. Chaikin, D. Hexner, E. J. Hinch, S. Ramaswamy, and H. Stone for helpful discussions. This research has been supported by the United States–Israel Binational Science Foundation (Grant No. 2012090).

*goldfriend@tau.ac.il
†hdiamant@tau.ac.il
‡t-witten@uchicago.edu

[1] S. Ramaswamy, Adv. Phys. **50**, 297 (2001).
[2] É. Guazzelli and J. Hinch, Annu. Rev. Fluid Mech. **43**, 97 (2011).
[3] R. Jean and L. Fan, in *Handbook of Fluid Dynamics*, 2nd ed., edited by R. W. Johnson (CRC Press, Boca Raton, FL, 2016) Chap. 20.3, pp. 20–80.
[4] J. Ham and G. Homsy, Int. J. Multiphase Flow **14**, 533 (1988).
[5] H. Nicolai and É. Guazzelli, Phys. Fluids **7**, 3 (1995).
[6] P. N. Segrè, E. Herbolzheimer, and P. M. Chaikin, Phys. Rev. Lett. **79**, 2574 (1997).
[7] P. Tong and B. J. Ackerson, Phys. Rev. E **58**, R6931 (1998).
[8] R. E. Caflisch and J. H. C. Luke, Phys. Fluids **28**, 759 (1985).
[9] A. J. C. Ladd, Phys. Rev. Lett. **76**, 1392 (1996).
[10] A. J. C. Ladd, Phys. Fluids **9**, 491 (1997).
[11] D. L. Koch, Phys. Fluids **6**, 2894 (1994).
[12] F. R. Cunha, G. C. Abade, A. J. Sousa, and E. J. Hinch, J. Fluids Eng. **124**, 957 (2002).
[13] L. Bergougnoux, S. Ghicini, É. Guazzelli, and J. Hinch, Phys. Fluids **15**, 1875 (2003).
[14] P. J. Mucha, S.-Y. Tee, D. A. Weitz, B. I. Shraiman, and M. P. Brenner, J. Fluid Mech. **501**, 71 (2004).
[15] D. L. Koch and E. S. G. Shaqfeh, J. Fluid Mech. **224**, 275 (1991).
[16] A. Levine, S. Ramaswamy, E. Frey, and R. Bruinsma, Phys. Rev. Lett. **81**, 5944 (1998).
[17] M. P. Brenner, Phys. Fluids **11**, 754 (1999).
[18] J. H. C. Luke, Phys. Fluids **12**, 1619 (2000).
[19] D. L. Koch and E. S. G. Shaqfeh, J. Fluid Mech. **209**, 521 (1989).
[20] A. A. Dahlkild, J. Fluid Mech. **689**, 183 (2011).
[21] P. Kumar and B. Ramarao, Chem. Eng. Commun. **108**, 381 (1991).
[22] M. A. Turney, M. K. Cheung, R. L. Powell, and M. J. McCarthy, AIChE J. **41**, 251 (1995).
[23] B. Herzhaft and É. Guazzelli, J. Fluid Mech. **384**, 133 (1999).
[24] B. Metzger, J. E. Butler, and É. Gauzzelli, J. Fluid Mech. **575**, 307 (2007).
[25] D. Saintillan, E. Darve, and E. S. G. Shaqfeh, Phys. Fluids **17**, 033301 (2005).
[26] J. E. Butler and E. S. G. Shaqfeh, J. Fluid Mech. **468**, 205 (2002).
[27] K. Gustavsson and A.-K. Tornberg, Phys. Fluids **21**, 123301 (2009).
[28] B. Cichocki, M. L. Ekiel-Jeżewska, G. Nägele, and E. Wajnryb, Phys. Fluids **23**, 083303 (2011).
[29] N. W. Krapf, T. A. Witten, and N. C. Keim, Phys. Rev. E **79**, 056307 (2009).
[30] T. Goldfriend, H. Diamant, and T. A. Witten, Phys. Fluids **27**, 123303 (2015).
[31] T. Goldfriend, H. Diamant, and T. A. Witten, Phys. Rev. E **93**, 042609 (2016).
[32] The situation for symmetric, nonaligning objects, such as spheroids, is more complicated since the unperturbed object does not have a well-defined orientation with the force [19].
[33] H. Nicolai, B. Herzhaft, E. Hinch, L. Oger, and E. Guazzelli, Phys. Fluids **7**, 12 (1995).
[34] R. Rusconi and H. A. Stone, Phys. Rev. Lett. **101**, 254502 (2008).
[35] Although a dipolar term of order a should be included in Eq. (2) to have a consistent expansion to first order in a, this divergenceless term has no effect on the results.
[36] C. Pozrikidis, *Boundary Integral and Singularity Methods for Linearized Viscous Flow* (Cambridge University Press, Cambridge, England, 1992).
[37] The mean-field assumption of constant Φ is valid provided that the motion of the isolated self-aligning object under an external force and flow gradient can be characterized by axisymmetric hydrodynamic tensors [38].
[38] See Supplemental Material at http://link.aps.org/supplemental/10.1103/PhysRevLett.118.158005 for more detailed analysis, which includes Refs. [39–45].
[39] S. Kim and S. J. Karrila, *Microhydrodynamics: Principles and Selected Applications* (Dover Publications, Mineola, NY, 2005).
[40] R. Cortez, L. Fauci, and A. Medovikov, Phys. Fluids **17**, 031504 (2005).

[41] J. Garcia de la Torre and B. Carrasco, Biopolymers **63**, 163 (2002).
[42] A. Filippov, J. Colloid Interface Sci. **229**, 184 (2000).
[43] O. Gonzalez, A. B. A. Graf, and J. H. Maddocks, J. Fluid Mech. **519**, 133 (2004).
[44] H. Brenner, Chem. Eng. Sci. **19**, 703 (1964).
[45] F. P. Bretherton, J. Fluid Mech. **14**, 284 (1962).
[46] Although this figure seems similar to the one drawn in Ref. [19] for symmetric, rodlike spheroids (which are not self-aligning), the scenarios are different. Whereas the rods are aligned by the flow lines, the ones depicted in Fig. 2(b) self-align with the force and are only perturbed by the flow lines.
[47] S. Torquato and F. H. Stillinger, Phys. Rev. E **68**, 041113 (2003).
[48] S. Torquato, Phys. Rev. E **94**, 022122 (2016).
[49] L. Corte, P. M. Chaikin, J. P. Gollub, and D. J. Pine, Nat. Phys. **4**, 420 (2008).
[50] J. H. Weijs, R. Jeanneret, R. Dreyfus, and D. Bartolo, Phys. Rev. Lett. **115**, 108301 (2015).
[51] D. Hexner and D. Levine, Phys. Rev. Lett. **114**, 110602 (2015).
[52] The one-component plasma [1,48] is another example of hyperuniformity brought about by long-ranged pair-interactions (electrostatic interactions in this case), falling off as $1/r$.
[53] N.-Q. Nguyen and A. J. Ladd, J. Fluid Mech. **525**, 73 (2005).
[54] X. Lei, B. J. Ackerson, and P. Tong, Phys. Rev. Lett. **86**, 3300 (2001).
[55] K. V. Kumar, Ph.D. thesis, Indian Institute of Science, 2010.